Epigenetic aging in a self-fertilizing vertebrate, the mangrove rivulus *Kryptolebias marmoratus*

Bélik Justine[1*], Silvestre Frédéric[1]

[1]Laboratory of Evolutionary and Adaptive Physiology, Institute of Life, Earth and Environment, University of Namur, Rue de Bruxelles, 61, Namur, Belgium

justine.belik@unamur.be (Corresponding author), frederic.silvestre@unamur.be

ABSTRACT

Background: Since Horvath (2013) and Hannum (2013), DNA methylation has emerged as a reliable biomarker for estimating age. Predictive models, called epigenetic clocks, are being built across the tree of life, including humans, other mammals and vertebrates and, recently, invertebrates. However, it always involves cross-fertilizing organisms, thus presenting a high level of genetic diversity. To decipher the exact role of epigenetics in adaptation and evolution, distinguishing true epigenetic variation from changes that reflect genetic variation is essential.

Results: Here, we used the mangrove rivulus, the only self-fertilizing vertebrate, to study epigenetic aging in the brain and construct an epigenetic clock. We generated a reduced representation bisulfite sequencing dataset of 90 brain tissues from individuals aged 60-1100 days to construct a highly accurate age predictor using 40 CpG sites ($R^2 > 0.96$, mean absolute error of 28.7 days). We associated the CpG sites with their respective closest genes and explored their biological functions. Genes relevant to aging include *lamin-A* (responsible for several age-related processes), aryl hydrocarbon receptor (whose absence causes premature aging) and several genes associated with Alzheimer's disease identified in human studies. We also propose several methods to improve classic epigenetic clock regression.

Conclusions: This study is the first construction of an epigenetic clock in a self-fertilizing species, demonstrating that DNA methylation patterns undergo consistent changes across the lifespan of isogenic individuals. These findings emphasize putative changes in DNA methylation related to functional changes across aging in the brain.

Keywords: DNA methylation, aging, mangrove rivulus, RRBS, elastic net regression, brain.

BACKGROUND

Aging is a progressive, time-dependent decline in physiological integrity, leading to impaired function and an increased risk of death among most living organisms [3–5]. It is considered the primary risk factor for several major human pathologies, including cancer, diabetes, cardiovascular disorders and neurodegenerative diseases, highlighting its central role in ongoing scientific research. López-Otín et al. [4] initially described nine "Hallmarks of Aging": genomic instability, telomere attrition, epigenetic alterations, loss of proteostasis, deregulated nutrient sensing, mitochondrial dysfunction, cellular senescence, stem cell exhaustion, and altered intercellular communication. These hallmarks have been widely studied and validated. However, the list has since been updated to include disabled macroautophagy, chronic inflammation, and dysbiosis [6]. Each hallmark represents a distinct yet interconnected entry point for investigating the biology of aging, as they collectively influence and reinforce one another.

Among the hallmarks of aging, epigenetic alterations play a significant role. These include changes in DNA methylation patterns, abnormal posttranslational modifications of histones, aberrant chromatin remodeling, and deregulated functions of noncoding RNAs [6]. Such modifications can profoundly impact gene expression, contributing to the onset and progression of several age-related pathologies. In particular, the age-associated accumulation of DNA methylation (DNAm) modifications has been extensively studied [7]. DNAm involves the addition of a methyl group to a cytosine, most commonly at CpG dinucleotides in vertebrates (i.e., a cytosine located 5' of a guanine). This process is achieved by a set of enzymes from the DNA methyltransferase (DNMT) family, notably, DNMT1 (which copies preexisting DNA methylation motifs onto the new strand during mitosis) and DNMT3a/3b (which perform *de novo* methylation). DNAm can be reversed through two primary processes: active demethylation, which is mediated by ten-eleven translocases (TETs) dioxygenases, and passive demethylation, which occurs when functional DNMT activity is absent during DNA replication [8].

Current literature demonstrates that aging is strongly correlated with DNAm, with substantial functional consequences. Early studies suggested that global genomic hypomethylation is a hallmark of aging [9–11]. However, more recent studies using advanced sequencing technologies have produced conflicting results and do not support this hypothesis [12–14]. Instead, age-related modifications of DNAm occur at specific regions and sites of the genome, and these alterations are often tissue- and species-specific [15]. Despite the variability, several recent studies agree that the normal DNA methylation landscape progressively erodes. This includes hypermethylation of previously unmethylated regions and hypomethylation of previously methylated regions, increasing the overall entropy of the DNAm pattern over time [16–18]. However, some CpG sites exhibit a strong, consistent correlation with chronological age, emphasizing their potential as age predictors [19]. These so-called "clock CpGs" form the basis of epigenetic clocks, sets of carefully selected loci across the genome that are collectively capable of predicting chronological age with high accuracy [20].

Key epigenetic clocks include the model developed by Horvath [1], constructed from 8,000 human multi-tissue samples, which uses 353 CpGs to estimate age with a median error of 3.6 years. The Hannum clock [2], which is based solely on human blood samples, highlights specific components of human aging. Levine et al. [21] advanced the concept of biological age *versus* chronological age by incorporating clinical health biomarkers into the clock's design. In parallel, numerous epigenetic clocks have been built across the tree of life. In mammals, examples include *Mus musculus* [22,23] and *Canis lupus familiaris* [24]. In birds, clocks have been constructed for *Gallus gallus* [25] and *Coturnix japonica* [26]. Clocks also exist for reptiles, such as *Alligator mississippiens* [27], and fish, including *Danio rerio* [28] and the European seabass [29]. In addition, the first epigenetic clocks for invertebrate species are now emerging [30,31]. The recent development of a universal pan-mammalian clock suggests that epigenetic aging is evolutionarily conserved across mammals [32]. Similarly, a study on cetaceans introduced a multi-species, two-tissue clock, highlighting the potential to develop tools applicable across diverse taxa [33].

The further development of epigenetic clocks is valuable, as it offers insights into aging mechanisms and related diseases. Comparative studies can identify universal and species-specific aspects of aging and epigenetic regulation [34]. Moreover, several independent studies have demonstrated that epigenetic age is indicative of past and/or present health status [35]. Epigenetic clocks offer yet underexploited potential in the context of breeding programs and fisheries management [20], as well as conservation work [36]. Age estimation notably enables the calculation of growth rates (to assess species productivity and growth variation over time), mortality rates (natural and fishing mortality rates) and age classes [20].

Most epigenetic clocks are based on easily accessible tissues, such as blood or caudal fins, to enable nonlethal and minimally invasive age estimation [20,29]. However, these tissues may not be the most relevant for increasing our fundamental understanding of aging. In contrast, investigating the aging brain methylome is critically important, given its influence on neural function and the development of neurodegenerative diseases [37–40]. Only a few epigenetic clocks have been constructed via postmortem brain samples, either in nonhuman primates [41,42] or humans [43,44]. To our knowledge, only two studies have focused on the brain in the context of the epigenetic clock [23,45]. Thus, expanding our knowledge of brain-specific methylation patterns in the context of aging has become an essential objective for both epigenetic and neuroscience research.

Here, we focus on *Kryptolebias marmoratus,* the only self-fertilizing vertebrate with its sister species, *Kryptolebias hermaphroditus*. Commonly known as the mangrove rivulus, it belongs to a broad group of killifish species and is distributed along the coasts of Florida to northern Brazil, closely following the red mangrove *Rhizophora mangle* [46]. Its reproduction strategy is remarkable, as it involves a rare mixed mating system known as androdioecy [47]. Populations of *K. marmoratus* are composed of self-fertilizing hermaphrodites, which produce clonal offspring after a few generations, and males, which can cross-fertilize unfertilized eggs laid by hermaphrodites. In natural populations, there is a gradient in male frequency, resulting in varying

levels of genetic diversity, with selfing rates ranging from 49 to 97% [48]. The population used in our study originates from Emerson Point Preserve, Florida, and is characterized by an extremely high selfing rate of 97% and an observed heterozygosity of zero. The virtual absence of genetic variation offers a unique opportunity to study epigenetic variation without the confounding effects of underlying genetic differences.

We used 90 brain samples of hermaphrodite *K. marmoratus* of known age, which were evenly distributed across its life span (from 60 days to 3.5 years after hatching). We performed a Reduced Representation Bisulfite Sequencing (RRBS) and found and identified 40 CpG sites whose methylation levels collectively predict age, with a median absolute error of 28.7 days (R^2 of 0.96). The locations of the sites in the genome were investigated, and each site was associated with the gene in which it was located or, if not, the closest gene. Several of these genes are involved in aging-related processes (dsDNA damage repair, mTOR signaling, inflammation, autophagy, etc.) as well as processes involved in Alzheimer's disease (AD). This study demonstrated that DNA methylation patterns undergo dynamic changes across the lifespan, even in the absence of genetic variation.

RESULTS

Age-associated CpG sites identified by RRBS

Information about the fish used (Fish ID, Age at death and Length) are in Table S1. *The bisulfite conversion was 98.87%. RRBS samples were aligned to the K. marmoratus reference genome, with an average alignment rate of 56.8%. The percentage of global methylation was 60.2%. Global methylation did not significantly correlate with age (p value = 0.5748, Figure S1).*

The first model was constructed using all individuals. A total of 467,182 CpG sites were common to all individuals, with a minimum coverage of 15 and maximum coverage set at the 99.9th percentile. Among these sites, 36,704 CpGs were significantly correlated with age (correlation test, corrected for multiple testing via the Benjamini-Hochberg procedure). The selected regression has an alpha value of 0.1 and a lambda value of 0.05. This model achieved an R^2 of 0.938. However, as the correlation was less accurate in older individuals (**Figure 1A**), the model was rerun using only individuals younger than 900 days (76 individuals). A total of 475,502 CpG sites were common to these individuals, with a minimum coverage of 15 and maximum coverage set at the 99.9th percentile. Among these sites, 29,126 were significantly correlated with age (correlation test, corrected for multiple testing via the Benjamini–Hochberg procedure). The selected regression has an alpha value of 0.1 and a lambda value of 0.150.

To build an efficient aging tool, the number of predictors must be minimized while sufficient predictive power must be maintained. The final model included 40 CpG sites and achieved an R^2 of 0.960 (**Figure 1B**). Validation of the model by Leave-One-Out-Cross-Validation (LOOCV) yielded virtually identical results, indicating that both approaches capture true accuracy equally well. A MAE of 28.7 days was found in the testing dataset, and no statistical difference was observed

between the absolute error rate between the training and testing data sets (p-value = 0.066, welch-test, two-tailed) (**Figure 1C**).

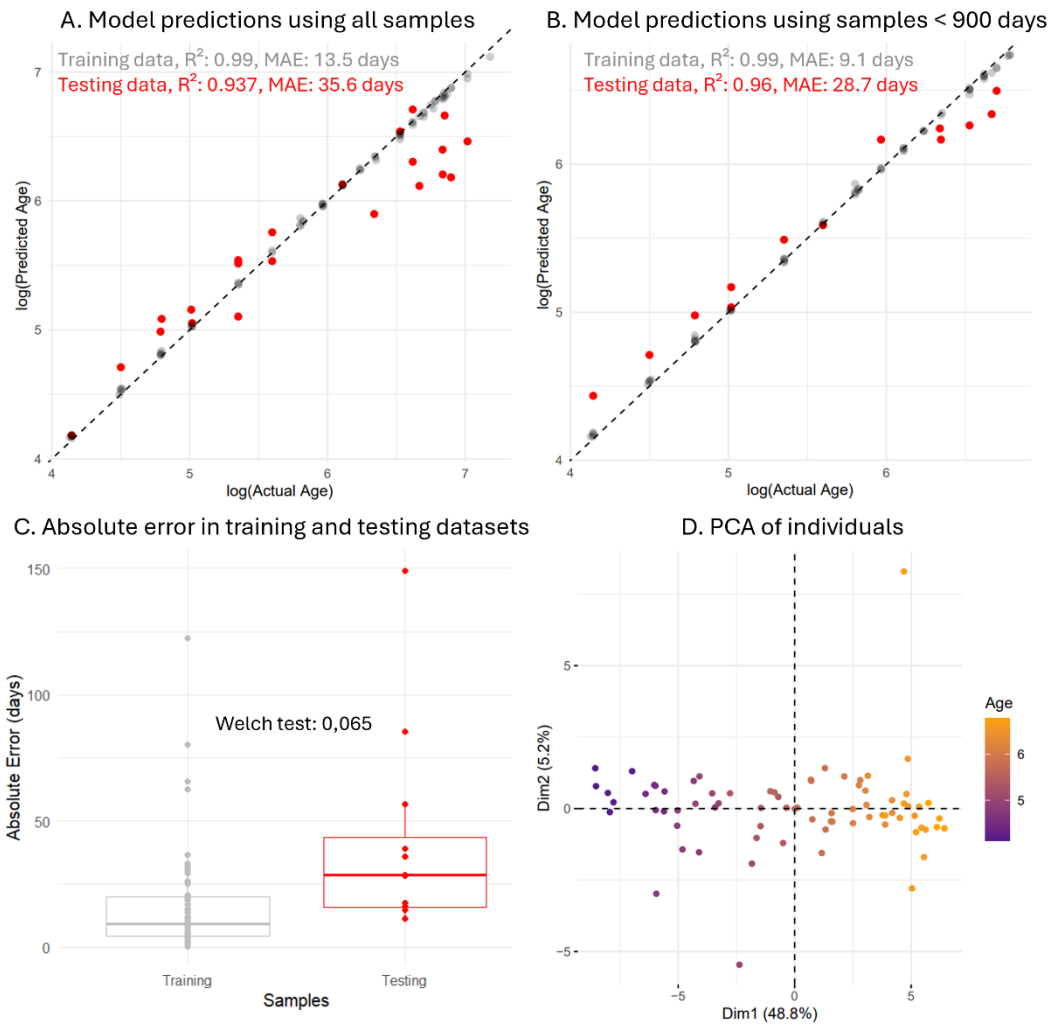

Figure 1: Mangrove rivulus age estimation. Chronological age is plotted against predicted age, for both training (in gray) and testing (in red) datasets, with respective R^2 and MAE, for both all individuals (A) and individuals younger than 900 days only (B). Absolute Error for both training and testing datasets, for the regression excluding the older individuals, with Welch-test (C). PCA of individuals using the 40 CpG sites, showing a clear separation based on age in the first principal component (D).

We subsequently performed a PCA of the individuals (**Figure 1D**), with chronological age represented as a color gradient. The first principal component explained 48.8% of the total variance and was strongly associated with age. The second component explained 5.2% of the total variance.

Identification and characterization of age-related CpG sites

Information for each CpG site and its associated gene is summarized in **Table 1**. Among the 40 selected CpG sites, 31 showed an increase in the percentage of methylation with age, whereas 9 exhibited a decrease. Among these sites, 31 were located within gene bodies, 8 were positioned upstream (ranging from 232 to 5,622 base pairs from the start codon), and 1 was located

downstream (11,307 base pairs). Each gene was evaluated for methylation level changes (DNAm change), strength of association (R^2), genomic context, distance to the gene if not within it, and functional relevance (Table 1). The methylation percentages of each CpG site with age are shown in Figure S2.

Table 1: Chromosome and position, Distance to the gene, R^2 and DNA methylation change (from 60 DPH to 900 DPH), Gene name and ID and Biological Significance using Z-fin.

Chr, position	Distance	R^2, DNAm change	Gene name and ID	Biological significance (Z-fin)
Chr1, 9323024	1291	0,566 13% → 40%	gnb1l Guanine nucleotide-binding protein subunit beta-like protein 1 ZDB-GENE-050320-77	Involved in cell cycle progression, signal transduction, apoptosis, and gene regulation.
Chr1, 10730302	0	0,546 42% → 72%	msi1b musashi RNA binding protein 1b ZDB-GENE-050320-86	Enable mRNA binding activity.
Chr2, 7418712	0	0,475 40% → 78%	synrg synergin ZDB-GENE-030131-9396	Part of clathrin coat of trans-Golgi network vesicle.
Chr3, 14648133	0	0,683 20% → 53%	lrba LPS-responsive vesicle trafficking, beach and anchor containing ZDB-GENE-090311-19	Enable protein kinase binding activity. Involved in protein localization.
Chr4, 11103886	0	0,267 12% → 25%	hyal1 hyaluronidase 1 ZDB-GENE-060312-42	Enable hyalurononglucosaminidase activity. Involved in hyaluronan catabolic process.
Chr5, 1055068	0	0,28 25% → 40%	lmna lamin A ZDB-GENE-020424-3	Structural constituent of cytoskeleton.
Chr5, 6018182	0	0,214 10% → 30%	skiv2l Ski2-like RNA Helicase ZDB-TSCRIPT-100915-49	Enable RNA helicase activity. Involved in nuclear-transcribed mRNA catabolic process, 3'-5' exonucleolytic nonsense-mediated decay.
Chr5, 10638440	0	0,423 5% → 18%	klhl38a kelch-like family member 38a ZDB-GENE-060503-737	Enable ubiquitin-like ligase-substrate adaptor activity. Involved in proteasome-mediated ubiquitin-dependent protein catabolic process. Part of Cul3-RING ubiquitin ligase complex.
Chr6, 181223	0	0,378 62% → 35%	TTN Titin	Structural constituent of muscle. Acts upstream of or within several

			ZDB-GENE-030616-413	processes, including heart contraction and striated muscle tissue development.
Chr6, 2171690	0	0,34 95% → 77%	cops8 COP9 signalosome subunit 8 ZDB-GENE-040426-982	Act upstream of or within COP9 signalosome assembly and protein deneddylation.
Chr6, 2171717	0	0,214 98% → 88%		
Chr6, 19162718	232	0,513 47% → 76%	Ahr aryl hydrocarbon receptor ZDB-GENE-990714-16	Enables nuclear receptor activity and sequence-specific DNA binding activity. Acts upstream of or within several processes, including fin development; ovarian follicle development; and positive regulation of transcription by RNA polymerase II.
Chr8, 12560302	0	0,425 7% → 23%	IQSEC1 IQ motif and Sec7 domain ArfGEF 1 ZDB-GENE-120813-2	Enable guanyl-nucleotide exchange factor activity. Acts upstream of or within angiogenesis and lymphangiogenesis.
Chr8, 13059272	0	0,269 4% → 13%	plxnd1 plexin D1 ZDB-GENE-040426-1828	Enable semaphorin receptor activity. Acts upstream of or within with a negative effect on sprouting angiogenesis. Acts upstream of or within embryonic eye morphogenesis and vasculature development.
Chr10, 9160868	1174	0,413 10% → 30%	fermt2 FERM domain containing kindlin 2 ZDB-GENE-050506-132	Enable integrin binding activity. Acts upstream of or within cell migration; circulatory system development; and cytoskeleton organization.
Chr11, 12833818	0	0,437 52% → 27%	slc25a22a solute carrier family 25-member 22a ZDB-GENE-110408-61	Enable L-aspartate transmembrane transporter activity and L-glutamate transmembrane transporter activity.
Chr11, 12950935	0	0,537 13% → 33%	Saxo4/ppp1r32 stabilizer of axonemal microtubules 4 ZDB-GENE-120913-1	Enable phosphatase binding activity.
Chr11, 14053781	0	0,456 55% → 85%	otud7a OTU deubiquitinase 7A ZDB-GENE-100212-1	Enable DNA binding activity; cysteine-type deubiquitinase activity; and zinc ion binding activity.
Chr14, 2182519	0	0,589 7% → 25%	tfap2e transcription factor AP-2 epsilon ZDB-GENE-040426-1455	Enable DNA-binding transcription activator activity, RNA polymerase II-specific and RNA polymerase II transcription regulatory region sequence-specific DNA binding
Chr14, 2183494	0	0,608 25% → 55%		

				activity. Acts upstream of or within melanocyte differentiation.
Chr14, 7714032	5622	0,511 55% → 77%	myo18b myosin XVIIIB ZDB-GENE-111111-8	Acts upstream of or within sarcomerogenesis.
Chr15, 5068118	0	0,539 32% → 65%	cdh15 cadherin 15 ZDB-GENE-030131-780	Enable beta-catenin binding activity and cadherin binding activity. Involved in several processes, including calcium-dependent cell–cell adhesion via plasma membrane cell adhesion molecules; cell–cell adhesion mediated by cadherin; and cell–cell junction organization
Chr16, 10652845	0	0,618 60% → 13%	dbpb D site albumin promoter binding protein b ZDB-GENE-100922-6	Enable DNA-binding transcription factor activity, RNA polymerase II-specific and RNA polymerase II cis-regulatory region sequence-specific DNA binding activity. Involved in regulation of transcription by RNA polymerase II. Act upstream of or within regulation of DNA-templated transcription.
Chr16, 11363278	0	0,358 45% → 25%	itga10 integrin, alpha 10 ZDB-GENE-100922-54	Enable integrin binding activity. Involved in several processes, including cell adhesion mediated by integrin; cell-matrix adhesion; and integrin-mediated signaling pathway. Act upstream of or within cell adhesion.
Chr16, 14332044	673	0,627 5% → 30%	twist1b twist family bHLH transcription factor 1b ZDB-GENE-050417-357	Enable cis-regulatory region sequence-specific DNA binding activity. Acts upstream of or within several processes, including circulatory system development; pharyngeal system development; and regulation of bone mineralization.
Chr16, 29541652	0	0,562 67% → 35%	cep162 centrosomal protein 162 ZDB-GENE-100922-266	Involved in cilium assembly. Acts upstream of or within heart looping.
Chr17, 13385366	2958	0,615 22% → 50%	tut1 terminal uridylyl transferase 1, U6 snRNA-specific ZDB-GENE-050706-68	Enable enzyme-substrate adaptor activity; mRNA 3'-UTR binding activity; and nucleotidyltransferase activity.

				Involved in cotranscriptional mRNA 3'-end processing, cleavage and polyadenylation pathway and snRNA processing. Act upstream of or within mRNA processing.
Chr18, 15967531	998	0,652 56% → 85%	ascl4 Achaete-Scute Family BHLH Transcription Factor 4 MGI:1914591*	Enable DNA-binding transcription factor activity, RNA polymerase II-specific and RNA polymerase II transcription regulatory region sequence-specific DNA binding activity. Involved in regulation of transcription by RNA polymerase II. *
Chr19, 265466	0	0,777 30% → 72%	nkx2.4b NK2 homeobox 4b ZDB-GENE-000830-1	Enable DNA-binding transcription factor activity, RNA polymerase II-specific and RNA polymerase II cis-regulatory region sequence-specific DNA binding activity. Acts upstream of or within hypothalamus development and thyroid gland development.
Chr19, 265551	0	0,677 25% → 62%		
Chr19, 265783	0	0,489 45% → 75%		
Chr19, 15280333	2755	0,558 42% → 73%	peli2 pellino E3 ubiquitin protein ligase family member 2 ZDB-GENE-040718-360	Enable ubiquitin protein ligase activity. Predicted to be involved in protein polyubiquitination. Act upstream of or within regulation of Toll signaling pathway.
Chr20, 3209495	0	0,426 25% → 55%	jcad junctional cadherin 5 associated a ZDB-GENE-111221-2	Involved in positive regulation of blood vessel endothelial cell proliferation involved in sprouting angiogenesis.
Chr20, 10412132	-11307	0,584 30% → 60%	cdh2 cadherin 2, type 1, N-cadherin ZDB-GENE-990415-171	Enable beta-catenin binding activity; cadherin binding activity; and calcium ion binding activity. Involved in cell–cell adhesion and neural tube formation.
Chr20, 11307320	0	0,393 55% → 75%	tmem275 transmembrane protein 275 ZDB-GENE-131121-130	Located in membrane.
Chr21, 15660274	0	0,401 40% → 14%	map3k22 mitogen-activated protein kinase kinase kinase 22 ZDB-GENE-070928-11	Enable protein serine/threonine kinase activity. Involved in intracellular signal transduction. Act upstream of or within protein phosphorylation.
Chr22, 26875602	0	0,521 25% → 52%	Srfb serum response factor b	Enable DNA-binding transcription factor activity, RNA polymerase II specific; cis-regulatory region sequence-specific DNA binding

			ZDB-GENE-040426-1294	activity; and protein dimerization activity. Act upstream of or within positive regulation of transcription by RNA polymerase II.
Chr24, 12606753	0	0,467 0% → 17%	haus8 HAUS augmin like complex subunit 8 ZDB-GENE-030131-6830	Enable microtubule binding activity. Involved in centrosome cycle and spindle assembly.
Chr24, 12606769	0	0,547 0% → 35%		
Chr24, 24522970	0	0,275 50% → 30%	ltbp latent transforming growth factor beta binding protein ZDB-GENE-091202-8	Involved in transforming growth factor beta receptor signaling pathway. Acts upstream of or within several processes, including heart morphogenesis; regulation of smooth muscle tissue development; and smooth muscle cell proliferation.

* Not found on Z-fin. From NCBI, in *Mus musculus*

The five genes with the highest R^2 values are nkx2.4b (position 265466, R^2 of 0.777), lrba (R^2 of 0.683), nkx2.4b (position 265551, R^2 of 0.677), ascl4 (R^2 of 0.652) and dbpb (0.618). These five CpG sites show a switch in methylation percentage from 30 to 45%. Only dbpb shows a decrease in methylation with age (60% to 13%). The nkx2.4b gene appears twice in the 5 most correlated CpG, and a third CpG site present in this gene was also selected within our 40 CpG sites, with an R^2 of 0.489. Two CpG sites were also selected within the same gene for cops8 (R^2 values of 0.340 and 0.214, both decreasing methylation), haus8 (R^2 values of 0.547 and 0.467, both increasing methylation), and tfap2e (R^2 values of 0.608 and 0.589, both increasing methylation).

Among the genes found, several essential functions were identified. Notably, cell cycle progression, signal progression and apoptosis (gnb1l), mRNA binding activity (msi1b), mRNA 3'-end processing, cleavage and polyadenylation (tut1), protein kinase activity (lrba), cytoskeleton (lmna), structural component of muscle (titin), microtubule binding activity (haus8), DNA binding transcription activity (tfap2e, dbpb, nkx2.4b and srfb), serine/threonine kinase activity (map3k22) and transformation of the growth factor beta receptor signaling pathway (ltbp) were investigated. The complete list of gene roles associated with the selected CpG sites can be found in Table 1.

DISCUSSION

Although a substantial body of research has explored epigenetic clocks, they predominantly use mammalian models and focus on peripheral tissues such as blood or skin (e.g., [1,21,23,24,41,49,50]). The vast amount of data on mammals has made it possible to construct a pan-mammalian epigenetic clock, which encompasses 59 tissue types in 185 mammalian species and predicts age with high accuracy ($r > 0.96$) [32]. However, applications to brain tissue remain scarce and, to our knowledge, have been studied only in humans [18,51,52], macaques

[41] and mice [53]. Similarly, no studies have examined epigenetic aging in self-fertilizing vertebrate species. Here, we present the first study to examine non-pathological brain aging in a self-fertilizing vertebrate species, the mangrove rivulus. *K. marmoratus* has an androdioecious mating system composed of self-fertilizing hermaphrodites and males [47]. The presence of naturally isogenic lineage makes this species a unique opportunity to subtract genetic noise and focus on epigenetic variation. In this study, the aim was not only to define the epigenetic clock of a self-fertilizing vertebrate but also to study the baseline epigenetic aging of the brain. Using 90 individuals aged 60-1100 days, which is the main lifespan of the mangrove rivulus, we conducted RRBS on the brain samples and selected 40 CpG sites whose methylation levels are collectively capable of predicting age with high accuracy ($R^2 > 0.96$) and a MAE of 28.7 days.

Four main technical optimizations were applied in this study. First, the effects of different training and testing data splits were tested, as prior work frequently employs ratios of 70–30, 75–25, or 80–20. All three configurations were evaluated via multiple random seeds (Table S2). The results consistently indicated that an 80–20 split yielded superior performance when measured on the testing dataset, as a larger training set provides the regression model with more data to learn from, thereby enhancing predictive accuracy. It is crucial to retain a sufficiently large test set to avoid artificially inflating the model performance. To further mitigate the risk of overfitting caused by favorable partitions, a 10-fold cross-validation was implemented, which offers a more robust estimate of the model's generalizability by assessing its performance across multiple training–testing splits within the training set. The training set is divided randomly into 10 parts, where 9 of them are used for training and the last is used for testing, and this procedure is repeated 10 times.

We also demonstrate that conducting an initial selection of CpG sites based on their individual correlation with chronological age is helpful for stabilizing the model. The vast majority of CpGs show no significant association with age; for example, out of 475,502 CpGs common across all individuals, only 29,126 remain after applying for a basic correlation test. Without this pre-filtering step, the final regression model tends to include CpG sites whose methylation levels are only minimally related to age. As the model processes nearly half a million CpGs, it increases the likelihood of incorporating weakly correlated sites by chance. While the overall predictive performance remains nearly identical, it is nonetheless advantageous to prioritize CpGs with strong individual correlations to age. This finding supports the broader view that age-related DNA methylation is not merely a product of epigenetic drift but reflects selected biological processes involving specific epigenetic features [54].

When constructing an age prediction tool, it is essential to identify the optimal balance between the number of CpG sites included and the predictive accuracy of the model. Because this relationship is non-linear, it must be carefully assessed to avoid unnecessary trade-offs. We recommend adjusting the threshold of inclusion importance for CpG sites in the regression to achieve precise and meaningful selection. Importantly, the model does not invariably benefit from adding more CpG sites, as increasing the number of predictors beyond the optimal point can reduce interpretability without improving performance.

Previous studies have demonstrated that epigenetic clocks tend to systematically underestimate chronological age in older individuals [55]. One explanation for this bias is the early saturation of methylation levels at selected CpG sites. For older individuals, the regression model may expect methylation values to surpass 100% or drop below 0%, which is biologically implausible and consequently reduces predictive reliability. Another contributing factor may be the presence of 5-hydroxymethylcytosine (5hmC), which cannot be distinguished from 5-methylcytosine (5mC) via conventional bisulfite sequencing methods, thereby distorting age predictions in tissues where 5hmC is abundant, such as the brain [55]. To our knowledge, the level of 5hmC in mangrove rivulus brain tissue has not been characterized. However, insights from other teleost fish suggest that hydroxymethylation plays an important regulatory role. In *Oreochromis niloticus*, differential hydroxymethylation has been observed in genes associated with growth, particularly within gene bodies and promoters [56]. Epigenetic drift, which is the alteration of the epigenomic landscape with age, might also impact the accuracy of the regression of older individuals [2,57]. The biological, functional, clinical and evolutionary significance of this epigenetic drift, however, remains unclear [58].

Among genes associated with the selected CpGs, several have attracted our attention in the study of aging. The CpG at position 1055068 on chromosome 5 is within the gene *lamin-A* (*lmna*) and shows hypermethylation with age (from 22% of methylation at 60 days to 40% at 900 days). *lmna* encodes the prelamin-A/C protein, which undergoes four post-translational steps to become mature lamin A, the main constituent of the nuclear lamina [59]. Defect in the post-translational maturation disrupt nuclear function and affect aging-related processes, such as mTOR signaling, epigenetic modifications, the stress response, inflammation, microRNA activation and mechanosignaling, causing premature aging syndromes such as Hutchinson–Gilford progeria syndrome [60]. Moreover, lamin A, which is typically not expressed in neurons, appears to transform from senile to AD neurons and contributes to halting the consequences of cell cycle re-entry and nuclear Tau exit, allowing the survival of the neuron. This irreversible nuclear transformation leads to neurofibrillary tangle formation and, ultimately, neurodegeneration [61].

A second CpG site of interest is located at position 19162718 on chromosome 6, 232 base pairs upstream from the gene *Aryl Hydrocarbon Receptor* (AhR). It shows hypermethylation with age, ranging from 47% to 77%. AhR is a ligand-dependent transcription factor that is classically associated with the regulation of xenobiotic metabolism in response to environmental toxicants [62]. Several AhR ligands, such as resveratrol and quercetin, have been shown to extend the lifespan of model organisms [63–65]. However, conflicting results have been obtained, depending on the ligand, species, and experimental setup used [66,67]. It has also been suggested that AhR reveals evidence of antagonistic pleiotropy in the regulation of the aging process, i.e., the gene is beneficial during development but shows deleterious properties during aging [68].

Two selected CpG sites are within *cops8* (COP9 signalosome 8) and are both hypomethylated with age (position 2171690, ranging from 98% methylation to 77%, and position 2171717, ranging from 98% to 87%). The COP9 signalosome participates in several cellular and developmental

processes in various eukaryotic organisms and is associated with de-ubiquitination and protein kinase activities [69]. Subunit 8 is a central regulator of the proteasomal proteolytic pathway and selective autophagy [70]. The autophagic–lysosomal pathway is critical for the removal of oxidized proteins in the heart [71]. Like epigenetic alterations, impaired autophagy is one of the primary hallmarks of aging [6].

Among the other selected CpGs, several show a link with AD. A Genome Wide Association study revealed that FERM domain containing kindlin 2 (*fermt2)* (CpG 1174 base pair upstream, which is upregulated with age) is a locus susceptible to AD. These results suggested that *ferm2* modulates AD risk by regulating APP metabolism and Aβ peptide production [72]. Another GWAS revealed that an increased risk of developing AD has been associated with 27 genes, including fermt2. LPS-responsive vesicle trafficking, beach and anchor containing (*Lrba*), solute carrier family 25-member 22a (*slc25A22*) and integrin alpha 10 (*itga10*) are differentially expressed in AD patients compared with healthy cognitive adults and have been found in our epigenetic clock [73–75].

Our research identified markers of baseline aging in the brain of the mangrove rivulus, which are also associated with age-related diseases in humans. Although we have focused on CpGs associated with genes that have been linked in the literature to aging and/or neurodegeneration, it is important to study the mechanism of other CpGs in the future. A particular focus should be placed on the nkx2.4b, haus8 and tfap2e genes, for which several CpGs have been selected. These genes may have an underestimated role in the aging and death of individuals, but no literature has mentioned them. Exploring these candidates not only broadens our understanding of potential contributors to aging but also provides an opportunity to investigate how their alteration may drive or protect against disease processes. In this context, studying baseline brain aging has revealed genes associated with human pathologies, highlighting the value of experimentally disrupting these markers to characterize the resulting pathological consequences. Such disruption can be achieved through exposure to neurotoxins or through genetic and epigenetic modifications such as CRISPR-Cas9 and CRISPR-dCas9 [76–79].

The selected CpG sites and the sequencing data generated add to the data already available for other teleost species, e.g., zebrafish [28], European sea bass [80], scorpion fish [81], and cow nose rays [82], all of which show very high accuracy. The increasing number of studies on the teleost epigenetic clock has increased interest in the construction of a pan-teleost epigenetic clock, similar to the high accuracy of its construction for mammals, which includes 185 species and 59 tissue types [32]. This first pan-epigenetic clock proposes solutions to solve the inconstancy in sequencing methods, different lifespans, etc., underlying the feasibility of such a general epigenetic clock. The development of a common epigenetic clock for all teleost species would be particularly valuable in the fields of aquaculture and conservation [20].

The epigenetic clock constructed in this study opens many avenues for future research. The 40 selected CpG sites can be used as tools for determining the age of mangrove rivulus. From this perspective, a robust and cost-efficient method is the amplification of target regions from bisulfite-

converted DNA, followed by a second PCR to generate libraries for Illumina NGS [83]. This epigenetic clock was built on a naturally highly isogenic population (Emerson Point Preserve, Florida). However, other populations exist and present different levels of genetic diversity [48]. The application of our work to other populations could be used to evaluate whether the predictive accuracy holds across broader genetic backgrounds. From a similar perspective, the aging tool could be applied to wild populations. This method would provide valuable ecological information by enabling the estimation of age structures in natural populations, thereby deepening our understanding of demographic processes and life history traits [20].

A transformative approach in aging research is the development of biological epigenetic clocks, which estimate age on the basis of physiological and/or molecular characteristics instead of relying solely on chronological age [84]. Contrasting biological and chronological age can reveal valuable insights into the health and aging trajectories of populations, highlighting patterns such as accelerated or decelerated aging that may signal environmental stressors or distinctive physiological states [85–87]. Applying biological age assessments to fish opens new possibilities for conservation by providing more precise evaluations of population health. Integrating these molecular age estimates with ecological information, such as information on pollution and climate variation, allows for a more nuanced understanding of how environmental factors impact wild fish populations.

CONCLUSION

Our study not only revealed age-related changes in CpG methylation patterns but also represents the first development of an epigenetic clock in a self-fertilizing vertebrate, the mangrove rivulus. This unique model allows the study of DNAm changes without the confounding effects of genetic variation, providing insights into the specific roles of DNAm in aging. Using brain tissue enabled us to investigate baseline aging processes in this organ and to gain functional insights into brain aging. The genes identified here warrant further investigation to improve our understanding of brain aging and its links to neurodegenerative diseases.

MATERIAL AND METHODS

Mangrove rivulus aging colony

Kryptolebias marmoratus individuals were collected in 2019 from Emerson Point Preserve, Florida (N25°01’45.64”, W80°29’49.24”, permit number SAL-24-1132**A**-SR) and used to establish the F0 generation at the University of Namur. The fish were individually housed in 500 mL plastic containers filled with 300 mL of 12 ± 1 parts per thousand (ppt) saltwater (Instant Ocean™ Sea salt) and maintained in a climate-controlled room at 25 ± 1°C under a 12:12 light:dark photoperiod. The fish were fed daily *ad libitum* with live *Artemia salina*.

For the epigenetic clock analysis, only hermaphrodites were selected. These fish ranged in age from 60-1100 days post-hatching (dph) and were between the 2nd and 6th generations derived from the F0 stock. A total of 96 fish were initially selected; however, four were excluded after being identified as secondary males, and two were removed because of insufficient DNA yield. Once they reached the expected age, the fish were euthanized by rapid cooling (immersion in water between 0°C and 4°C for 20 seconds), and death was confirmed by decapitation. Each individual was photographed, measured and weighed. Detailed information on individual fish is provided in Supplementary Table S1. All procedures were approved by the animal ethics committee of the University of Namur (UN PM KE 23/020). Following euthanasia, brain, liver, gonad and fin tissues were collected and stored at -80°C until DNA extraction.

DNA extraction

DNA was extracted using NucleoSpin Tissue XS kit (Marcherey-Nagel, item number 740901.250), with slight modifications to the manufacturer's protocol. An additional wash step, identical to the first, was included, and a 5-minute incubation at 37°C was added following the binding buffer step. Elution buffer was performed using 2x10 µL (instead of once 20 µL), with each followed by centrifugation at 11,000 × *g* for 1 minute. DNA quality and quantity were assessed via both a NanoDrop spectrophotometer and a high-intensity Qubit fluorimeter. Samples that did not meet the minimum amount of DNA required for the Diagenode RRBS kit (< 50 ng of DNA, see below) were excluded from further analyses (two samples in total).

Reduced-Representation Bisulfite Sequencing

RRBS libraries were prepared via the Premium RRBS Kit V2 from Diagenode (catalog number C02030037) following the manufacturer's protocol. This kit includes all the reagents required for enzymatic digestion, library preparation, bisulfite conversion and PCR amplification. The final DNA concentrations were determined via a high-sensitivity Qubit fluorimeter. Libraries were sequenced on a NovaSeq 6000 V1.5 (300 cycles XP workflow) with paired-end sequencing (20 million reads each way) via the GIGA platform (University of Liège, Belgium). The FASTQ files were quality checked via FastQC v0.11.8 (https://www.bioinformatics.babraham.ac.uk/projects/fastqc/).

Bioinformatics and methylation analysis

RAW FASTQ files were trimmed using *Trim Galore!* (version 0.6.10) with the following parameters: -rrbs -quality 28 -illumina -stringency 2 -length 40. Genome indexing and bisulfite alignment were performed via *Bismark* (version 0.24.1). The reference genome used was *Kryptolebias marmoratus*, whose latest version from NCBI (GCF_001649575.2_ASM164957v2) was prepared via Bismark_genome_preparation. Read alignment was conducted via Bowtie2 through bismark with the following parameters: -score_min L,0, 0.6. *SAMtools* (version 1.17) was then used to sort and index the resulting BAM files.

The files were then processed in R (version 4.2.2) via the *methylKit* (version 1.28.0) and *caret* (version 6.0-94) packages. Bam files were processed with *processBismarkAln* via assembly = ASM164957v2 and read.context = "CpG". Coverage filtering was applied via *filterByCoverage*, which retained only sites with a minimum coverage of 15 and maximum coverage below 99.9th percentile to mitigate PCR bias.

Predicting age from CpG methylation

The model was built and validated following the main steps shown in **Figure 2**. The CpGs present in all the samples were first selected using *methylKit::unite*. *percMethylation* function was used to create the percentage methylation matrix. The first selection of CpGs was carried out by correlating each CpG with the logarithm of the age of the individuals (*cor.test*, with Benjamini–Hochberg correction). Age was transformed to a natural log to fit a linear model. Preselecting the CpG stabilizes the sites selected in the final model when several seeds are compared.

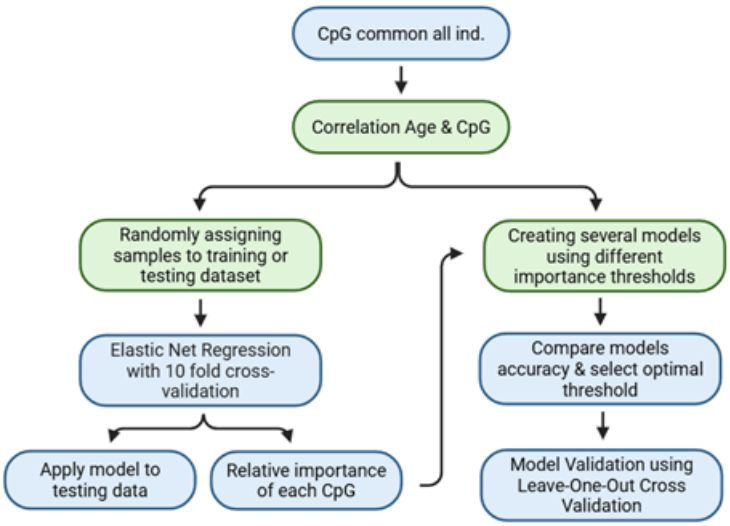

Figure 2: diagram of the main stages in building and validating the model. The green frames are steps that have been studied and optimized. Their conclusions are discussed in the materials and methods section.

The samples were randomly assigned to either a training (80%) or a testing dataset (20%) via the *createDataPartition* function in the caret R package. This division is necessary to prevent false improvements in model predictions. We tested the most common division, 70-30, 75-25 and 80-20, and compared the model accuracy with three different seeds. The 80–20 partition always provided the best results (Figure S1).

We used the *training* function from the *caret* package with 10-fold cross-validation to perform elastic net regression on the training dataset. This function tests the combination of three α (0.1, 0.5 and 1) and λ (depending on the data, always between 0 and 1) values. It selects the combination best suited to the data, i.e., the one with the highest R^2 (strength of linear relationship between chronological and predicted age) and lowest Median Absolute Error (MAE, precision of the

predictions). The selected model is then applied to the testing dataset, and both metrics are calculated.

This model assigns a relative importance value to each CpG (value between 0 and 100), which is used to reduce the number of CpGs included in the model. We applied an importance threshold so that only CpGs with relative importance above this threshold were included in the model. First, we performed a general screening, testing thresholds from 5-75, in steps of 5. To select the optimal model (our criterion was $R^2 > 0.95$ with the minimum number of CpGs), we performed a second screening of importance from 25-35 in steps of 1 to capture as much variability as possible. The final model was selected based on the strength and accuracy of the predictions from the testing dataset. We stress the importance of looking in detail at the different thresholds and their accuracy. The relationship between the number of predictors and the quality of predictions is not linear, highlighting the (non)complementarity of certain CpG subsets. For example, the performance of the model at threshold 41 is poorer than that at threshold 42, even though the latter model has one fewer CpG (not shown).

The model was ultimately evaluated using Leave-One-Out Cross Validation (LOOCV), where each fold consists of a single observation. In this approach, the model is trained on all data points except one, which is then used for testing. This process is repeated systematically so that every observation serves once as the test set. LOOCV provides an estimate of the true test error, as training is always performed on the full dataset minus one sample (James et al., 2013). The results revealed no difference between the model's performance and its validation.

Principal Component Analysis (PCA)

PCA was performed using the *FactoMineR* package (version 2.10), to visualize the individuals with respect to their age.

Biological significance

A file containing the chromosome, start and stop positions, and strand information for each selected CpG site was imported into SeqMonk (version 1.481) and analyzed using the genome assembly ASM164957v2 [88]. Probes were generated by assigning CpG sites to genes located within a maximum distance of 20,000 base pairs. The resulting annotation file included, in addition to the imported data, the associated gene name (*Features*), the Feature Orientation (upstream, overlapping, downstream, or null), and the distance between the CpG site and the gene when not overlapping. The roles of the genes were described via Z-fins to maintain consistency in the annotations.

DECLARATIONS

Ethics approval and consent to participate

All procedures were approved by the animal ethics committee of the University of Namur (UN PM KE 23/020).

Consent for publication

Not applicable

Availability of data and materials

The datasets generated and/or analysed during the current study are available in the NCBI repository, under the ID *BioProject ID PRJNA1331489*.

Competing interests

The authors declare that they have no competing interests

Funding

This research did not receive any specific grant from funding agencies in the public, commercial, or non-profit sectors.

Authors' contributions

JB conceptualized the article, generated and analysed the data and wrote the manuscript. FS reviewed and edited the manuscript and did validation and supervision. All authors read and approved of the final manuscript.

BIBLIOGRAPHY

1. Horvath S. DNA methylation age of human tissues and cell types. Genome Biology. 2013;14:3156.

2. Hannum G, Guinney J, Zhao L, Zhang L, Hughes G, Sadda S, et al. Genome-wide Methylation Profiles Reveal Quantitative Views of Human Aging Rates. Molecular Cell. 2013;49:359–67.

3. Jones MJ, Goodman SJ, Kobor MS. DNA methylation and healthy human aging. Aging Cell. 2015;14:924–32.

4. López-Otín C, Blasco MA, Partridge L, Serrano M, Kroemer G. The Hallmarks of Aging. Cell. 2013;153:1194–217.

5. Rose M, Flatt T, Graves Jr JL, Greer LF, Martínez DE, Matos M, et al. What is Aging? Front Genet [Internet]. 2012 [cited 2025 Aug 14];3. Available from: https://www.frontiersin.org/journals/genetics/articles/10.3389/fgene.2012.00134/full

6. López-Otín C, Blasco MA, Partridge L, Serrano M, Kroemer G. Hallmarks of aging: An expanding universe. Cell. 2023;186:243–78.

7. Seale K, Horvath S, Teschendorff A, Eynon N, Voisin S. Making sense of the ageing methylome. Nat Rev Genet. 2022;23:585–605.

8. Davletgildeeva AT, Kuznetsov NA. The Role of DNMT Methyltransferases and TET Dioxygenases in the Maintenance of the DNA Methylation Level. Biomolecules. 2024;14:1117.

9. Fuke C, Shimabukuro M, Petronis A, Sugimoto J, Oda T, Miura K, et al. Age Related Changes in 5-methylcytosine Content in Human Peripheral Leukocytes and Placentas: an HPLC-based Study. Annals of Human Genetics. 2004;68:196–204.

10. Singhal RP, Mays-Hoopes LL, Eichhorn GL. DNA methylation in aging of mice. Mechanisms of Ageing and Development. 1987;41:199–210.

11. Wilson VL, Smith RA, Ma S, Cutler RG. Genomic 5-methyldeoxycytidine decreases with age. Journal of Biological Chemistry. 1987;262:9948–51.

12. Fasolino M, Liu S, Wang Y, Zhou Z. Distinct cellular and molecular environments support aging-related DNA methylation changes in the substantia nigra. Epigenomics. 2017;9:21–31.

13. Lister R, Mukamel EA, Nery JR, Urich M, Puddifoot CA, Johnson ND, et al. Global Epigenomic Reconfiguration During Mammalian Brain Development. Science. 2013;341:1237905.

14. Raddatz G, Hagemann S, Aran D, Söhle J, Kulkarni PP, Kaderali L, et al. Aging is associated with highly defined epigenetic changes in the human epidermis. Epigenetics & Chromatin. 2013;6:36.

15. Unnikrishnan A, Hadad N, Masser DR, Jackson J, Freeman WM, Richardson A. Revisiting the genomic hypomethylation hypothesis of aging. Annals of the New York Academy of Sciences. 2018;1418:69–79.

16. Meyer DH, Schumacher B. Aging clocks based on accumulating stochastic variation. Nat Aging. 2024;4:871–85.

17. Tarkhov AE, Lindstrom-Vautrin T, Zhang S, Ying K, Moqri M, Zhang B, et al. Nature of epigenetic aging from a single-cell perspective. Nat Aging. 2024;4:854–70.

18. Tong H, Dwaraka VB, Chen Q, Luo Q, Lasky-Su JA, Smith R, et al. Quantifying the stochastic component of epigenetic aging. Nat Aging. 2024;4:886–901.

19. De Paoli-Iseppi R, Deagle BE, McMahon CR, Hindell MA, Dickinson JL, Jarman SN. Measuring Animal Age with DNA Methylation: From Humans to Wild Animals. Frontiers in Genetics [Internet]. 2017 [cited 2022 Nov 28];8. Available from: https://www.frontiersin.org/articles/10.3389/fgene.2017.00106

20. Piferrer F, Anastasiadi D. Age estimation in fishes using epigenetic clocks: Applications to fisheries management and conservation biology. Front Mar Sci [Internet]. 2023 [cited 2024 May 24];10. Available from: https://www.frontiersin.org/articles/10.3389/fmars.2023.1062151

21. Levine ME, Lu AT, Quach A, Chen BH, Assimes TL, Bandinelli S, et al. An epigenetic biomarker of aging for lifespan and healthspan. Aging (Albany NY). 2018;10:573–91.

22. Spiers H, Hannon E, Wells S, Williams B, Fernandes C, Mill J. Age-associated changes in DNA methylation across multiple tissues in an inbred mouse model. Mechanisms of Ageing and Development. 2016;154:20–3.

23. Stubbs TM, Bonder MJ, Stark A-K, Krueger F, Bolland D, Butcher G, et al. Multi-tissue DNA methylation age predictor in mouse. Genome Biology. 2017;18:68.

24. Thompson MJ, vonHoldt B, Horvath S, Pellegrini M. An epigenetic aging clock for dogs and wolves. Aging. 2017;9:1055–68.

25. Gryzinska M, Blaszczak E, Strachecka A, Jezewska-Witkowska G. Analysis of Age-Related Global DNA Methylation in Chicken. Biochem Genet. 2013;51:554–63.

26. Andraszek K, Gryzińska M, Wójcik E, Knaga S, Smalec E. Age-Dependent Change in the Morphology of Nucleoli and Methylation of Genes of the Nucleolar Organizer Region in Japanese Quail (Coturnix japonica) Model (Temminck and Schlegel, 1849) (Galliformes: Aves). Folia Biologica. 2014;62:293–300.

27. Nilsen FM, Parrott BB, Bowden JA, Kassim BL, Somerville SE, Bryan TA, et al. Global DNA methylation loss associated with mercury contamination and aging in the American alligator (Alligator mississippiensis). Science of The Total Environment. 2016;545–546:389–97.

28. Mayne B, Korbie D, Kenchington L, Ezzy B, Berry O, Jarman S. A DNA methylation age predictor for zebrafish. Aging (Albany NY). 2020;12:24817–35.

29. Piferrer F, Miska EA, Anastasiadi D. Chapter 10 - Epigenetics in fish evolution. In: Guerrero-Bosagna CM, editor. On Epigenetics and Evolution [Internet]. Academic Press; 2024 [cited 2025 Aug 14]. p. 283–306. Available from: https://www.sciencedirect.com/science/article/pii/B9780443190513000103

30. Brink K, Thomas C, Jones A, Mallon E. An epigenetic clock in an insect model system.

31. Guynes K, Sarre LA, Carrillo-Baltodano AM, Davies BE, Xu L, Liang Y, et al. Annelid methylomes reveal ancestral developmental and aging-associated epigenetic erosion across Bilateria. Genome Biol. 2024;25:204.

32. Lu AT, Fei Z, Haghani A, Robeck TR, Zoller JA, Li CZ, et al. Universal DNA methylation age across mammalian tissues. Nat Aging. 2023;3:1144–66.

33. Zoller JA, Lu AT, Haghani A, Horvath S, Robeck T. Enhancing epigenetic aging clocks in cetaceans: accurate age estimations in small endangered delphinids, killer whales, pilot whales, belugas, humpbacks, and bowhead whales. Sci Rep. 2025;15:4048.

34. Bertucci-Richter EM, Parrott BB. The rate of epigenetic drift scales with maximum lifespan across mammals. Nat Commun. 2023;14:7731.

35. Caulton A, Dodds KG, McRae KM, Couldrey C, Horvath S, Clarke SM. Development of Epigenetic Clocks for Key Ruminant Species. Genes. 2022;13:96.

36. Heydenrych MJ, Saunders BJ, Bunce M, Jarman SN. Epigenetic Measurement of Key Vertebrate Population Biology Parameters. Front Ecol Evol [Internet]. 2021 [cited 2025 Aug 14];9. Available from: https://www.frontiersin.org/journals/ecology-and-evolution/articles/10.3389/fevo.2021.617376/full

37. Liu L, van Groen T, Kadish I, Tollefsbol TO. DNA methylation impacts on learning and memory in aging. Neurobiology of Aging. 2009;30:549–60.

38. Pellegrini C, Pirazzini C, Sala C, Sambati L, Yusipov I, Kalyakulina A, et al. A Meta-Analysis of Brain DNA Methylation Across Sex, Age, and Alzheimer's Disease Points for Accelerated Epigenetic Aging in Neurodegeneration. Front Aging Neurosci [Internet]. 2021 [cited 2025 May 15];13. Available from: https://www.frontiersin.org/journals/aging-neuroscience/articles/10.3389/fnagi.2021.639428/full

39. Thrush KL, Bennett DA, Gaiteri C, Horvath S, Dyck CH van, Higgins-Chen AT, et al. Aging the brain: multi-region methylation principal component based clock in the context of Alzheimer's disease. Aging. 2022;14:5641–68.

40. Yang J, Yu L, Gaiteri C, Srivastava GP, Chibnik LB, Leurgans SE, et al. Association of DNA methylation in the brain with age in older persons is confounded by common neuropathologies. Int J Biochem Cell Biol. 2015;67:58–64.

41. Horvath S, Zoller JA, Haghani A, Jasinska AJ, Raj K, Breeze CE, et al. Epigenetic clock and methylation studies in the rhesus macaque. GeroScience. 2021;43:2441–53.

42. Jasinska AJ, Haghani A, Zoller JA, Li CZ, Arneson A, Ernst J, et al. Epigenetic clock and methylation studies in vervet monkeys. GeroScience. 2021;44:699–717.

43. Grodstein F, Lemos B, Yu L, Klein H-U, Iatrou A, Buchman AS, et al. The association of epigenetic clocks in brain tissue with brain pathologies and common aging phenotypes. Neurobiology of Disease. 2021;157:105428.

44. Shastri GG, Sudre G, Ahn K, Jung B, Kolachana B, Auluck PK, et al. Cortico-striatal differences in the epigenome in attention-deficit/ hyperactivity disorder. Transl Psychiatry. 2024;14:189.

45. Coninx E, Chew YC, Yang X, Guo W, Coolkens A, Baatout S, et al. Hippocampal and cortical tissue-specific epigenetic clocks indicate an increased epigenetic age in a mouse model for Alzheimer's disease. Aging (Albany NY). 2020;12:20817–34.

46. Taylor DS. Twenty-Four Years in the Mud: What Have We Learned About the Natural History and Ecology of the Mangrove Rivulus, Kryptolebias marmoratus? Integrative and Comparative Biology. 2012;52:724–36.

47. Costa WJEM, Lima SMQ, Bartolette R. Androdioecy in Kryptolebias killifish and the evolution of self-fertilizing hermaphroditism. Biol J Linn Soc. 2010;99:344–9.

48. Chapelle V. Adaptation and evolution with low genetic diversity: a combined field and laboratory study on DNA methylation variation in the mangrove rivulus Kryptolebias marmoratus. 2023.

49. Horvath S, Haghani A, Zoller JA, Raj K, Sinha I, Robeck TR, et al. Epigenetic clock and methylation studies in marsupials: opossums, Tasmanian devils, kangaroos, and wallabies. Geroscience. 2022;44:1825–45.

50. Robeck TR, Haghani A, Fei Z, Lindemann DM, Russell J, Herrick KES, et al. Multi-tissue DNA methylation aging clocks for sea lions, walruses and seals. Commun Biol. 2023;6:359.

51. Horvath S, Mah V, Lu AT, Woo JS, Choi O-W, Jasinska AJ, et al. The cerebellum ages slowly according to the epigenetic clock. Aging (Albany NY). 2015;7:294–306.

52. Shireby GL, Davies JP, Francis PT, Burrage J, Walker EM, Neilson GWA, et al. Recalibrating the epigenetic clock: implications for assessing biological age in the human cortex. Brain. 2020;143:3763–75.

53. Meer MV, Podolskiy DI, Tyshkovskiy A, Gladyshev VN. A whole lifespan mouse multi-tissue DNA methylation clock. Kaeberlein M, Tyler JK, Wagner W, Adams P, editors. eLife. 2018;7:e40675.

54. Bertucci EM, Parrott BB. Is CpG Density the Link between Epigenetic Aging and Lifespan? Trends in Genetics. 2020;36:725–7.

55. El Khoury LY, Gorrie-Stone T, Smart M, Hughes A, Bao Y, Andrayas A, et al. Systematic underestimation of the epigenetic clock and age acceleration in older subjects. Genome Biol. 2019;20:283.

56. Konstantinidis I, Sætrom P, Fernandes JMO. Genome-wide hydroxymethylation profiles in liver of female Nile tilapia with distinct growth performance. Sci Data. 2023;10:114.

57. Heyn H, Li N, Ferreira HJ, Moran S, Pisano DG, Gomez A, et al. Distinct DNA methylomes of newborns and centenarians. Proceedings of the National Academy of Sciences. 2012;109:10522–7.

58. Teschendorff AE, West J, Beck S. Age-associated epigenetic drift: implications, and a case of epigenetic thrift? Hum Mol Genet. 2013;22:R7–15.

59. Lin F, Worman HJ. Structural organization of the human gene encoding nuclear lamin A and nuclear lamin C. Journal of Biological Chemistry. 1993;268:16321–6.

60. Cenni V, Capanni C, Mattioli E, Schena E, Squarzoni S, Bacalini MG, et al. Lamin A involvement in ageing processes. Ageing Research Reviews. 2020;62:101073.

61. Gil L, Niño SA, Capdeville G, Jiménez-Capdeville ME. Aging and Alzheimer's disease connection: Nuclear Tau and lamin A. Neuroscience Letters. 2021;749:135741.

62. Hankinson O. The Aryl Hydrocarbon Receptor Complex. Annual Review of Pharmacology and Toxicology. 1995;35:307–40.

63. Bhullar KS, Hubbard BP. Lifespan and healthspan extension by resveratrol. Biochimica et Biophysica Acta (BBA) - Molecular Basis of Disease. 2015;1852:1209–18.

64. Kampkötter A, Timpel C, Zurawski RF, Ruhl S, Chovolou Y, Proksch P, et al. Increase of stress resistance and lifespan of *Caenorhabditis elegans* by quercetin. Comparative Biochemistry and Physiology Part B: Biochemistry and Molecular Biology. 2008;149:314–23.

65. Pietsch K, Saul N, Menzel R, Stürzenbaum SR, Steinberg CEW. Quercetin mediated lifespan extension in Caenorhabditis elegans is modulated by age-1, daf-2, sek-1 and unc-43. Biogerontology. 2009;10:565–78.

66. Eckers A, Jakob S, Heiss C, Haarmann-Stemmann T, Goy C, Brinkmann V, et al. The aryl hydrocarbon receptor promotes aging phenotypes across species. Sci Rep. 2016;6:19618.

67. Serna E, Verdú D, Valls A, Belenguer-Varea Á, Tarazona-Santabalbina FJ, Borrás C, et al. Involvement of Aryl Hydrocarbon Receptor in Longevity and Healthspan: Insights from Humans, Mice, and C. elegans. Int J Mol Sci. 2024;25:9943.

68. Salminen A. Aryl hydrocarbon receptor (AhR) reveals evidence of antagonistic pleiotropy in the regulation of the aging process. Cell Mol Life Sci. 2022;79:489.

69. Wei N, Deng XW. The COP9 Signalosome. Annual Review of Cell and Developmental Biology. 2003;19:261–86.

70. Su H, Li F, Ranek MJ, Wei N, Wang X. COP9 Signalosome Regulates Autophagosome Maturation. Circulation. 2011;124:2117–28.

71. Su H, Li J, Osinska H, Li F, Robbins J, Liu J, et al. The COP9 Signalosome Is Required for Autophagy, Proteasome-Mediated Proteolysis, and Cardiomyocyte Survival in Adult Mice. Circulation: Heart Failure. 2013;6:1049–57.

72. Chapuis J, Flaig A, Grenier-Boley B, Eysert F, Pottiez V, Deloison G, et al. Genome-wide, high-content siRNA screening identifies the Alzheimer's genetic risk factor FERMT2 as a major modulator of APP metabolism. Acta Neuropathol. 2017;133:955–66.

73. Kim B-H, Nho K, Huang Y-N, Risacher SL, Kim JP, Yi D, et al. Genome-wide association meta-analysis identifies a novel LRBA locus for brain age acceleration in two independent Korean Cohorts. Alzheimer's & Dementia. 2023;19:e082848.

74. Tian J, Jia K, Wang T, Guo L, Xuan Z, Michaelis EK, et al. Hippocampal transcriptome-wide association study and pathway analysis of mitochondrial solute carriers in Alzheimer's disease. Transl Psychiatry. 2024;14:1–15.

75. Zou C, Su L, Pan M, Chen L, Li H, Zou C, et al. Exploration of novel biomarkers in Alzheimer's disease based on four diagnostic models. Front Aging Neurosci [Internet]. 2023 [cited 2025 May 20];15. Available from: https://www.frontiersin.org/journals/aging-neuroscience/articles/10.3389/fnagi.2023.1079433/full

76. Cai R, Lv R, Shi X, Yang G, Jin J. CRISPR/dCas9 Tools: Epigenetic Mechanism and Application in Gene Transcriptional Regulation. International Journal of Molecular Sciences. 2023;24:14865.

77. Caobi A, Dutta RK, Garbinski LD, Esteban-Lopez M, Ceyhan Y, Andre M, et al. The Impact of CRISPR-Cas9 on Age-related Disorders: From Pathology to Therapy. Aging Dis. 2020;11:895–915.

78. Chen C-D, Zeldich E, Li Y, Yuste A, Abraham CR. Activation of the Anti-Aging and Cognition-Enhancing Gene Klotho by CRISPR-dCas9 Transcriptional Effector Complex. J Mol Neurosci. 2018;64:175–84.

79. Ruetz TJ, Pogson AN, Kashiwagi CM, Gagnon SD, Morton B, Sun ED, et al. CRISPR–Cas9 screens reveal regulators of ageing in neural stem cells. Nature. 2024;634:1150–9.

80. Anastasiadi D, Piferrer F. A clockwork fish: Age prediction using DNA methylation-based biomarkers in the European seabass. Molecular Ecology Resources. 2020;20:387–97.

81. Weber DN, Fields AT, Patterson WF, Barnett BK, Hollenbeck CM, Portnoy DS. Novel epigenetic age estimation in wild-caught Gulf of Mexico reef fishes. Can J Fish Aquat Sci. 2022;79:1–5.

82. Weber D, Wyffels JT, Buckner C, George R, Ed Latson F, LePage V, et al. Noninvasive, epigenetic age estimation in an elasmobranch, the cownose ray (Rhinoptera bonasus). Sci Rep. 2024;14:26261.

83. Albrecht C, Bashtrykov P, Jeltsch A. Amplicon-Based Bisulfite Conversion-NGS DNA Methylation Analysis Protocol. Methods Mol Biol. 2024;2842:405–18.

84. Levine M, McDevitt RA, Meer M, Perdue K, Di Francesco A, Meade T, et al. A rat epigenetic clock recapitulates phenotypic aging and co-localizes with heterochromatin. Suh Y, Tyler JK, Laird P, Schumacher B, editors. eLife. 2020;9:e59201.

85. Oblak L, van der Zaag J, Higgins-Chen AT, Levine ME, Boks MP. A systematic review of biological, social and environmental factors associated with epigenetic clock acceleration. Ageing Research Reviews. 2021;69:101348.

86. Gensous N, Sala C, Pirazzini C, Ravaioli F, Milazzo M, Kwiatkowska KM, et al. A Targeted Epigenetic Clock for the Prediction of Biological Age. Cells. 2022;11:4044.

87. Li A, Koch Z, Ideker T. Epigenetic aging: Biological age prediction and informing a mechanistic theory of aging. Journal of Internal Medicine. 2022;292:733–44.

88. Kelley JL, Yee M-C, Brown AP, Richardson RR, Tatarenkov A, Lee CC, et al. The Genome of the Self-Fertilizing Mangrove Rivulus Fish, *Kryptolebias marmoratus* : A Model for Studying Phenotypic Plasticity and Adaptations to Extreme Environments. Genome Biol Evol. 2016;8:2145–54.